Inorganic Chemistry
Article

Inorg. Chem. **2010**, *49*, 5811–5817 **5811**
DOI: 10.1021/ic9025206

Syntheses, Crystal and Electronic Structures, and Physical Properties of Quaternary Semiconductors: $Ln_2Mn_3Sb_4S_{12}$ (Ln = Pr, Nd, Sm, Gd)

Hua-Jun Zhao,[†,‡] Long-Hua Li,[†,‡] Li-Ming Wu,[†] and Ling Chen*[,†]

[†]*Key Laboratory of Optoelectronic Materials Chemistry and Physics, Fujian Institute of Research on the Structure of Matter, Chinese Academy of Sciences, Fuzhou, Fujian 350002, People's Republic of China, and* [‡]*Graduate School of the Chinese Academy of Sciences, Beijing 100039, People's Republic of China*

Received December 18, 2009

Four new quaternary lanthanide antimony sulfides: $Ln_2Mn_3Sb_4S_{12}$ (Ln = Pr, Nd, Sm, Gd) have been synthesized from a stoichiometric element mixture at 1373 K by conventional solid state reactions. These compounds crystallize in the monoclinic space group *C2/m* with the unit cell parameters of $a = 19.928(2)-19.9672(6)$ Å, $b = 3.9323(4)-3.8803(2)$ Å, $c = 14.921(2)-14.9011(1)$ Å, $V = 938.5(2)-925.63(6)$ Å^3, and $Z = 2$ on going from Ln = Pr to Gd. Their structure represents a novel wavy MnS_6 octahedron layer decorated on both sides by chains of an SbS_5 square pyramid via strong Sb−S bonding interactions (< 3.0 Å). Such a MnS_6 octahedron layer consists of chains of an edge-sharing $[Mn1S_6]_2$ dimer extending along [010] that are interconnected by single strings of an edge-sharing $Mn2S_6$ octahedron at axial S apexes. $Sm_2Mn_3Sb_4S_{12}$ displays spin-canted antiferromagnetic interactions between Sm^{2+} and Mn^{2+} centers and an optical gap of 1.50 eV. The DFT study indicates an indirect band gap with an electronic transfer excitation of S 3p to Sb 5p orbital electrons.

Introduction

Main group metal chalcogenides are interesting not only because of their potential application as thermoelectric materials, such as Sb_2Te_3,[1] $Ag_{1-x}Pb_{18}SbTe_{20}$,[2] $Mo_3Sb_5Te_2$,[3] and $AgSb_xBi_{3-x}S_5$,[4] and non-linear optical (NLO) materials, such as $AgGaQ_2$ (Q = S, Se),[5−7] $LiGaQ_2$ (Q = S, Se, Te),[8] $LiInQ_2$ (Q = S, Se),[9] $BaGa_4S_7$,[10] $K_2Hg_3Ge_2S_8$,[11] $Li_2Ga_2GeS_6$,[12] Li_2CdGeS_4,[13] and $ZnY_6Si_2S_{14}$,[14] but also because of their diverse structure chemistry, which arises partly from the various local coordination spheres centered by the main group metal. Take antimony, for instance, the polyhedra of 3-, 4-, 5-, and 6-fold coordinated SbQ_n (n = 3, 4, 5, 6; Q = chalcogenides) are the major local coordination motifs in the related compounds.[15−19] Moreover, the acentric group, SbS_3^{3-}, can induce noncentrosymmetric (NCS) structures, which may result in interesting physical properties, such as second-harmonic generation.[15,20−22]

Generally, A/Sb/Q (A = alkali metal; Q = chalcogenides) ternary or quaternary compounds have shown less dense Sb/Q

*To whom correspondence should be addressed. Tel: (011)86-591-83704947. E-mail: chenl@fjirsm.ac.cn.

(1) Thonhauser, T.; Scheidemantel, T. J.; Sofo, J. O.; Badding, J. V.; Mahan, G. D. *Phys. Rev. B* **2003**, *68*, 085201.
(2) Hsu, K.-F.; Loo, S.; Guo, F.; Chen, W.; Dyck, J. S.; Uher, C.; Hogan, T.; Polychroniadis, E. K.; Kanatzidis, M. G. *Science* **2004**, *303*, 818.
(3) Dashjav, E.; Szczepenowska, A.; Kleinke, H. *J. Mater. Chem.* **2002**, *12*, 345.
(4) Kim, J.-H.; Chung, D.-Y.; Bilc, D.; Loo, S.; Short, J.; Mahanti, S. D.; Hogan, T.; Kanatzidis, M. G. *Chem. Mater.* **2005**, *17*, 3606.
(5) Chemla, D. S.; Kupecek, P. J.; Robertson, D. S.; Smith, R. C. *Opt. Commun.* **1971**, *3*, 29.
(6) Willer, U.; Blanke, T.; Schade, W. *Appl. Opts.* **2001**, *40*, 5439.
(7) Bai, L.; Lin, Z.-S.; Wang, Z.-Z.; Chen, C. T. *J. Chem. Phys.* **2004**, *120*, 8772.
(8) (a) Isaenko, L.; Yelisseyev, A.; Lobanov, S.; Titov, A.; Petrov, V.; Zondy, J.-J.; Krinitsin, P.; Merkulov, A.; Vedenyapin1, V.; Smirnova, J. *Cryst. Res. Technol.* **2003**, *38*, 379. (b) Isaenko, L.; Krinitsin, P.; Vedenyapin1, V.; Yelisseyev, A.; Merkulov, A.; Zondy, J.-J.; Petrov, V. *Cryst. Growth Des.* **2005**, *5*, 1325.
(9) (a) Boyd, G. D.; Kasper, H. M.; McFee, J. H. *J. Appl. Phys.* **1973**, *44*, 2809. (b) Isaenko, L.; Yelisseyev, A.; Lobanov, S. *J. Appl. Phys.* **2002**, *91*, 9475.
(10) Lin, X.-S.; Zhang, G.; Ye, N. *Cryst. Growth Des.* **2009**, *9*, 1186.
(11) Liao, J. H.; Marking, G. M.; Hsu, K. F.; Matsushita, Y.; Ewbank, M. D.; Borwick, R.; Cunningham, P.; Rosker, M. J.; Kanatzidis, M. G. *J. Am. Chem. Soc.* **2003**, *125*, 9484.
(12) Kim, Y.; Seo, I.-S.; Martin, S. W.; Baek, J.; Halasyamani, P. S.; Arumugam, N.; Steinfink, H. *Chem. Mater.* **2008**, *20*, 6048.
(13) Lekse, J. W.; Moreau, M. A.; McNerny, K. L.; Yeon, J.; Halasyamani, P. S.; Aitken, J. A. *Inorg. Chem.* **2009**, *48*, 7516.
(14) Guo, S.-P.; Guo, G.-C.; Wang, M.-S.; Zou, J.-P.; Xu, G.; Wang, G.-J.; Long, S.-F.; Huang, J.-S. *Inorg. Chem.* **2009**, *48*, 7059.
(15) Gandrud, W. B.; Boyd, G. D.; Mcfee, J. H. *Appl. Phys. Lett.* **1970**, *16*, 59.
(16) Huang, F.-Q; Ibers, J. A. *J. Solid State Chem.* **2005**, *178*, 212.
(17) Assoud, A.; Kleinke, K. M.; Kleinke, H. *Chem. Mater.* **2006**, *18*, 1041.
(18) (a) Bente, K.; Edenharter, A. *Kristallogr.* **1989**, *186*, 31. (b) Pfitzner, A.; Kurowski, D. *Kristallogr.* **2000**, *215*, 373.
(19) Choi, K.-S.; Iordanidis, L.; Chondroudis, K.; Kanatzidis, M. G. *Inorg. Chem.* **1997**, *36*, 3804.
(20) Zhang, Q.; Chung, I.; Jang, J. I.; Ketterson, J. B.; Kanatzidis, M. G. *J. Am. Chem. Soc.* **2009**, *131*, 9896.
(21) Ye, N.; Chen, Q.; Wu, B.; Chen, C. T. *J. Appl. Phys.* **1998**, *84*, 555.
(22) Halasyamani, P. S.; Poeppelmeier, K. R. *Chem. Mater.* **1998**, *10*, 2753.

Published on Web 05/28/2010

substructures and wider energy gaps in comparison with binary Sb_2Q_3 because of the ionic A−Q bonding interactions. Examples are $K_2Ln_{2-x}Sb_{4+x}Se_{12}$,[23] $K_2Ln_2Sb_2Q_9$ (Ln = La, Gd; Q = S, Se),[24] and $Na_9Gd_5Sb_8S_{26}$.[25]

Recently, we reported the first quaternary $La_4FeSb_2S_{10}$[26] with a measured optical band gap of 1.00 eV. The theoretic study indicated that Fe atoms contributed around the Fermi level (E_F) so as to make the electronic transfer excitation from S 3p to Fe 3d orbital electrons and, thus, decrease the band gap with respect to either Sb_2S_3 (1.7−1.9 eV)[27] or La_2S_3 (1.7−2.0 eV).[28] And as expected, the band gap of $La_4FeSb_2S_{10}$ was smaller than that of alkali metal containing $K_2La_2Sb_2S_9$ (2.20 eV), in which the K−S ionic bonding interactions were involved.[24] Meanwhile, the band gap of $La_4FeSb_2S_{10}$ was also smaller than that of ternary $La_7Sb_9S_{24}$, ($Eg_{(cal)}$ = 1.55 eV on the basis of LMTO), whose La^{3+} cation only had a minor contribution to the conduction band and, thus, hardly influenced the band gap with respect to the binary Sb_2S_3.[17]

A simple composition comparison suggests that the structure and property differences between $La_4FeSb_2S_{10}$[26] and $La_7Sb_9S_{24}$[17] come from whether the transition metal (TM) Fe^{2+} ion is involved. In this paper, we report another novel example in such a Ln/TM/Sb/S family (Ln = lanthanide) to point out the coordination motif of TM and its connection, e.g., the FeS_4 tetrahedron versus MnS_6 octahedron, and determine the overall crystallographic structure to a considerable degree. And the physical property of the binary system, FeS (narrow band gap of 0.04 eV)[29] versus MnS (wide band gap of 3.2 eV),[30] leads to different properties of the quaternary products, for example, $La_4FeSb_2S_{10}$,[26] 1.00 eV, direct band gap versus $Sm_2Mn_3Sb_4S_{12}$, 1.50 eV, indirect band gap.

Regarding the ternary Mn/Sb/Q systems, rich structure chemistry has already been revealed. For instance, structure type dependencies on either the synthesis method in $MnSb_2S_4$[18] or the anionic combination in $MnSbQ_2X$ (Q = S, Se; X = Cl, Br, I) have been found.[31] The only known quaternary manganese antimony chalcogenide is $MnPb_4Sb_6S_{14}$,[32] which is composed of a $[Pb_4Sb_6S_{14}]^{2-}$ 3D network accommodating 1D chains of a MnS_6 octahedron. In this paper, we report the syntheses, crystal and electronic structures, and magnetic property and optical band gap of quaternary antimony sulfides: $Ln_2Mn_3Sb_4S_{12}$ (Ln = Pr, Nd, Sm, Gd).

Experimental Section

Synthesis. The elements were used as purchased and stored in a nitrogen-filled glovebox (moisture and oxygen level is less than 0.1 ppm), and all manipulations were performed inside the glovebox. Pr (99.5%), Nd (99.9%), Sm (99.9%), and Gd (99.95%) were purchased from Huhhot Jinrui Rare Earth Co., Ltd. S (99.999%) was purchased from Alfa Aesar China (Tianjin) Co., Ltd. The chunk of Mn (99.99%) was purchased from ABCR GmbH & Co. KG. and Sb (99.99%) from Sinopharm Chemical Reagent Co., Ltd. All reactants in evacuated fused-silicon tubes were placed in resistance furnaces with a controlled temperature.

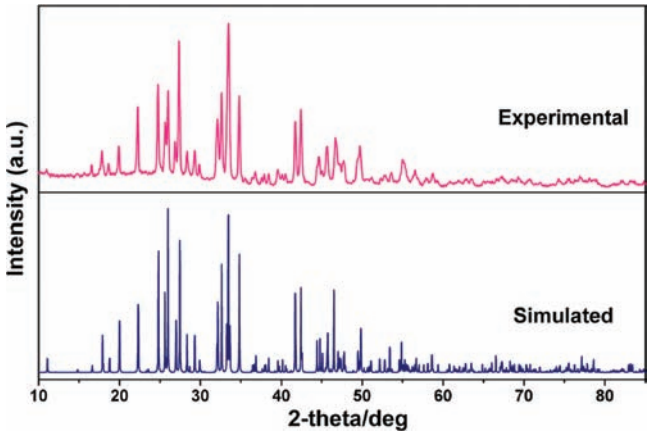

Figure 1. Experimental and simulated X-ray powder diffraction patterns of $Sm_2Mn_3Sb_4S_{12}$.

The first synthesis attempt started from elements with ratios of nominal $MnS/Ln_2S_3/Sb_2S_3$ = 1:1:1. The mixture of Ln, Mn, Sb, and S was weighed accordingly with an overall loading of about 300 mg and loaded into a silica tube, which was evacuated under a 10^{-3} Pa atmosphere and sealed. The samples were heated to 1100 °C over 36 h, kept at that temperature for 10 h, and subsequently cooled at 30 °C/h to 600 °C and annealed at this temperature for 393 h, and then the furnace was turned off. Dark red prism crystals were picked for single crystal structure analysis, which yielded a refined formula of $Ln_2Mn_3Sb_4S_{12}$ (Ln = Pr, Nd, Sm, Gd). The stoichiometry of $Pr_2Mn_3Sb_4S_{12}$ agrees well with the energy-dispersive X-ray spectroscopy (EDX) results of $Pr_2Mn_{2.4(3)}Sb_{3.9(3)}S_{12.3(8)}$ (Supporting Information, Figure S1) considering their intrinsically larger standard deviations. No other element, such as Si from the reaction container, was found. After the establishment of the formula, the title compounds can be synthesized from stoichiometric reactions. By this way, only $Sm_2Mn_3Sb_4S_{12}$ was produced as a single phased powder (Figure 1). The other three samples of $Ln_2Mn_3Sb_4S_{12}$ (Ln = Pr, Nd, Gd) contained Sb_2S_3 as a crystalline impurity (less than 40%). No reflection of lanthanide and manganese sulfides is observed. Efforts to obtain single phased products by annealing at 800 °C and slowly cooling (3 °C/h) from 1100 to 300 °C did not reduce the percentage of the Sb_2S_3 impurity. No corrosion on the silica tube in any case was observed, and all compounds are stable in the air for several months.

Crystal Structure Determinations. Data collections were performed on a Siemens Smart CCD diffractometer equipped with graphite-monochromated Mo Kα radiation (λ = 0.71073 Å) at 293 K. The data were corrected for Lorentz and polarization factors. Absorption corrections were performed by the SADABS program.[33] All structures were solved by direct methods and refined by full-matrix least-squares fitting on F^2 by SHELX-97.[34] All atoms were refined with anisotropic thermal parameters. All positions were fully occupied. Crystallographic data

(23) Chen, J. H.; Dorhout, P. K. *J. Alloys Compd.* **1997**, *249*, 199.
(24) Choi, K.-S.; Hanko, J. A.; Kanatzidis, M. G. *J. Solid State Chem.* **1999**, *147*, 309.
(25) Park, S.; Kim, S.-J. *J. Solid State Chem.* **2001**, *161*, 129.
(26) Zhao, H.-J.; Li, L.-H.; Wu, L.-M.; Chen, L. *Inorg. Chem.* **2009**, *48*, 11518.
(27) Shutov, S. D.; Sobolev, V. V.; Popov, Y. V.; Shestatskii, S. N. *Phys. Status Solidi* **1969**, *31*, K23.
(28) Gschneidner, K. A., J.; Beaudry, B. J.; Takeshita, T.; Eucker, S. S.; Taher, S. M. A.; Ho, J. C. *Phys. Rev. B* **1981**, *24*, 7187.
(29) Gosselin, J. R.; Townsend, M. G.; Trembly, R. J. *Solid State Commun.* **1976**, *19*, 799.
(30) Kan, S. H.; Felner, I.; Banin, U. *Israel J. Chem.* **2001**, *41*, 55.
(31) (a) Tougait, O.; Ibers, J. A.; Mar, A. *Acta Crystallogr., Sect. C* **2003**, *59*, i77. (b) Doussier, C.; Leone, P.; Moelo, Y. *Solid State Sci.* **2004**, *6*, 1387. (c) Doussier, C.; Moelo, Y.; Leone, P. *Solid State Sci.* **2006**, *8*, 652.
(32) Léone, P.; Leuch, L. M.; Palvadeau, P.; Molinié, P.; Moëlo, Y. *Solid State Sci.* **2003**, *5*, 771.
(33) (a) Sheldrick, G. M. *SADABS*; University of Göttingen: Göttingen, Germany, 1996. (b) *CrystalClear*, version 1.3.5; Rigaku Corp.: The Woodlands, TX, 1999.
(34) Sheldrick, G. M. *SHELXTL*, version 5.1; Bruker-AXS: Madison, WI, 1998.

Table 1. Crystallographic Data and Refinement Details for $Ln_2Mn_3Sb_4S_{12}$

formula	$Pr_2Mn_3Sb_4S_{12}$	$Nd_2Mn_3Sb_4S_{12}$	$Sm_2Mn_3Sb_4S_{12}$	$Gd_2Mn_3Sb_4S_{12}$
fw	1318.36	1325.01	1337.34	1351.04
crystal system	monoclinic	monoclinic	monoclinic	monoclinic
crystal color	dark red	dark red	dark red	dark red
Z	2	2	2	2
space group	$C2/m$ (No. 12)	$C2/m$ (No. 12)	$C2/m$ (No. 12)	$C2/m$ (No. 12)
a (Å)	19.928(2)	19.94(1)	19.878(4)	19.9672(6)
b (Å)	3.9323(4)	3.915(2)	3.9026(7)	3.8803(2)
c (Å)	14.921(2)	14.93(1)	14.875(3)	14.9011(1)
α (deg)	90	90	90	90
β (deg)	126.620(0)	126.626(8)	126.628(2)	126.702(2)
γ (deg)	90	90	90	90
V (Å^3)	938.5(2)	934.6(1)	926.1(3)	925.63(6)
F(000)	1178	1182	1190	1198
D_c (g cm^{-3})	4.665	4.709	4.795	4.847
μ (mm^{-1})	14.111	14.407	15.920	16.102
$2\theta_{max}$ (deg)	51.36	49.98	51.42	51.40
GOF on F^2	1.116	1.059	1.091	1.064
R_1, wR_2 ($I > 2\sigma(I)$)[a]	0.0483, 0.1054	0.0420, 0.0942	0.0529, 0.1114	0.0456,0.1075
R_1, wR_2 (all data)	0.0546, 0.1094	0.0439, 0.0955	0.0660, 0.1200	0.0557,0.1152
diff peak, hole (e. Å^{-3})	4.468, −3.797	5.044, −3.283	4.073, −1.9892	4.419, −3.007

[a] $R_1 = \sum||F_o| - |F_c||/\sum|F_o|$, $wR_2 = [\sum w(F_o^2 - F_c^2)^2/\sum w(F_o^2)^2]^{1/2}$.

Table 2. Atomic Coordinates and Equivalent Isotropic Displacement Parameters of $Pr_2Mn_3Sb_4S_{12}$

atom	symmetry	x	y	z	U_{eq}[a]
Pr	4*i*	0.23956(6)	0	0.13413(8)	0.0157(3)
Sb1	4*i*	0.10573(8)	0	0.5499(1)	0.0297(4)
Sb2	4*i*	0.46508(9)	0	0.1909(1)	0.0303(4)
Mn1	4*i*	0.1999(2)	0	0.3793(2)	0.0172(6)
Mn2	2*a*	0	0	0	0.0232(9)
S1	4*i*	0.0584(3)	0	0.1974(3)	0.0148(9)
S2	4*i*	0.6020(2)	0	0.0228(3)	0.0114(8)
S3	4*i*	0.8315(2)	0	0.1069(3)	0.0119(8)
S4	4*i*	0.4115(3)	0	0.3488(3)	0.0139(8)
S5	4*i*	0.2552(2)	0	0.7061(3)	0.0127(8)
S6	4*i*	0.3477(3)	0	0.5508(4)	0.0169(9)

[a] U_{eq} is defined as one third of the trace of the orthogonalized U_{ij} tensor.

and structural refinement details are summarized in Table 1; the positional coordinates and isotropic equivalent thermal parameters for $Pr_2Mn_3Sb_4S_{12}$ are given in Table 2. Those for the other compounds are given in the Supporting Information. Important bond distances are listed in Table 3.

X-Ray Powder Diffraction. The homogeneity of samples was assessed by powder X-ray diffraction. The XRD pattern was collected on a Rigaku DMAX 2500 diffractometer at a scanning rate of 1°/min over 2θ ranging from 10 to 85°. The measured XRD pattern for $Sm_2Mn_3Sb_4S_{12}$ is in good agreement with the simulated one from crystal structure data (Figure 1).

Elemental Analysis. The elemental analyses of Pr, Mn, Sb, and S have been examined with the aid of a field emission scanning electron microscope (FESEM, JSM6700F) equipped with an energy dispersive X-ray spectrometer (EDX, Oxford INCA).

Magnetic Susceptibility. The DC (direct current) magnetic susceptibility of $Sm_2Mn_3Sb_4S_{12}$ was performed on a Quantum Design PPMS-9T magnetometer in the temperature range of 2−300 K. The X-ray pure polycrystalline sample was ground to a fine power to minimize possible anisotropic effects and loaded into a gelatin capsule. The data were corrected for the susceptibility of the container and for the diamagnetic contribution from the ion core. The susceptibility data in the temperature range 60−300 K were fit by a least-squares method to the Curie−Weiss equation $\chi_M = C/(T - \theta)$, where χ_M is the magnetic susceptibility, C is the Curie constant, and θ is the Weiss constant.

Table 3. Selected Bond Lengths (Å) of $Ln_2Mn_3Sb_4S_{12}$

	$Pr_2Mn_3Sb_4S_{12}$	$Nd_2Mn_3Sb_4S_{12}$	$Sm_2Mn_3Sb_4S_{12}$	$Gd_2Mn_3Sb_4S_{12}$
Ln−S2 × 2	2.951(3)	2.942(3)	2.917(4)	2.925(3)
Ln−S3 × 2	2.876(3)	2.862(3)	2.838(4)	2.829(3)
Ln−S3	2.977(4)	2.967(4)	2.941(5)	2.933(4)
Ln−S4	2.984(4)	2.969(4)	2.953(5)	2.927(4)
Ln−S5 × 2	3.044(3)	3.028(3)	3.016(4)	2.996(3)
Sb1−S5	2.454(4)	2.454(4)	2.448(5)	2.460(4)
Sb1−S4 × 2	2.625(3)	2.617(3)	2.618(3)	2.609(3)
Sb1−S6 × 2	2.940(3)	2.943(1)	2.930(4)	2.929(3)
Sb2−S2	2.621(4)	2.587(4)	2.617(5)	2.559(4)
Sb2−S1 × 2	2.668(3)	2.655(3)	2.650(4)	2.635(3)
Sb2−S3 × 2	2.923(3)	2.915(3)	2.900(4)	2.908(3)
Mn1−S1	2.487(5)	2.488(4)	2.486(6)	2.495(5)
Mn1−S6	2.497(5)	2.506(5)	2.511(6)	2.503(5)
Mn1−S6 × 2	2.651(3)	2.640(3)	2.644(4)	2.630(3)
Mn1−S5 × 2	2.767(3)	2.776(3)	2.775(4)	2.780(4)
Mn2−S1 × 2	2.437(4)	2.432(4)	2.430(5)	2.429(4)
Mn2−S2 × 4	2.699(3)	2.702(3)	2.705(3)	2.711(3)

The effective magnetic moment (μ_{eff}) was calculated from the equation $\mu_{eff} = (7.997C)^{1/2}\,\mu_B$.[35]

UV/vis Diffuse Reflectance Spectroscopy. The optical diffuse reflectance spectrum of $Sm_2Mn_3Sb_4S_{12}$ powder was measured at room temperature using a Perkin-Elmer Lambda 900 UV−vis spectrophotometer equipped with an integrating sphere attachment and $BaSO_4$ as a reference. The absorption spectrum was calculated from the reflection spectrum via the Kubelka−Munk function: $\alpha/S = (1 - R)^2/2R$, in which α is the absorption coefficient, S is the scattering coefficient, and R is the reflectance.[36]

Electronic Structure Calculations. Spin-polarized electronic structure calculations of $Sm_2Mn_3Sb_4S_{12}$ were performed with the highly accurate full-potential linear augmented plane wave plus local orbital (FPLAPW + LO) method within density-functional theory (DFT),[37−39] implemented in the WIEN2K program package.[40] The Perdew−Burke−Ernzerhof generalized

(35) O'Connor, C. J. *Prog. Inorg. Chem.* **1982**, *29*, 203.
(36) Kortüm, G. *Reflectance Spectroscopy*; Springer-Verlag: New York, 1969.
(37) Yu, R.; Krakauer, H.; Singh, D. *Phys. Rev. B* **1991**, *43*, 6411.
(38) Wimmer, E.; Krakauer, H.; Weinert, M.; Freeman, A. J. *Phys. Rev. B*. **1981**, *24*, 864.
(39) Mattheiss, L. F.; Hamann, D. R. *Phys. Rev. B* **1986**, *33*, 823.
(40) Blaha, P.; Schwarz, K.; Madsen, G. K.; Kvasnicka, D.; Luitz, J. *WIEN2k. An Augmented Plane WaVe + Local Orbitals Program for Calculating Crystal Properties*; Techn. Universität Wien: Vienna, Austria, 2001.

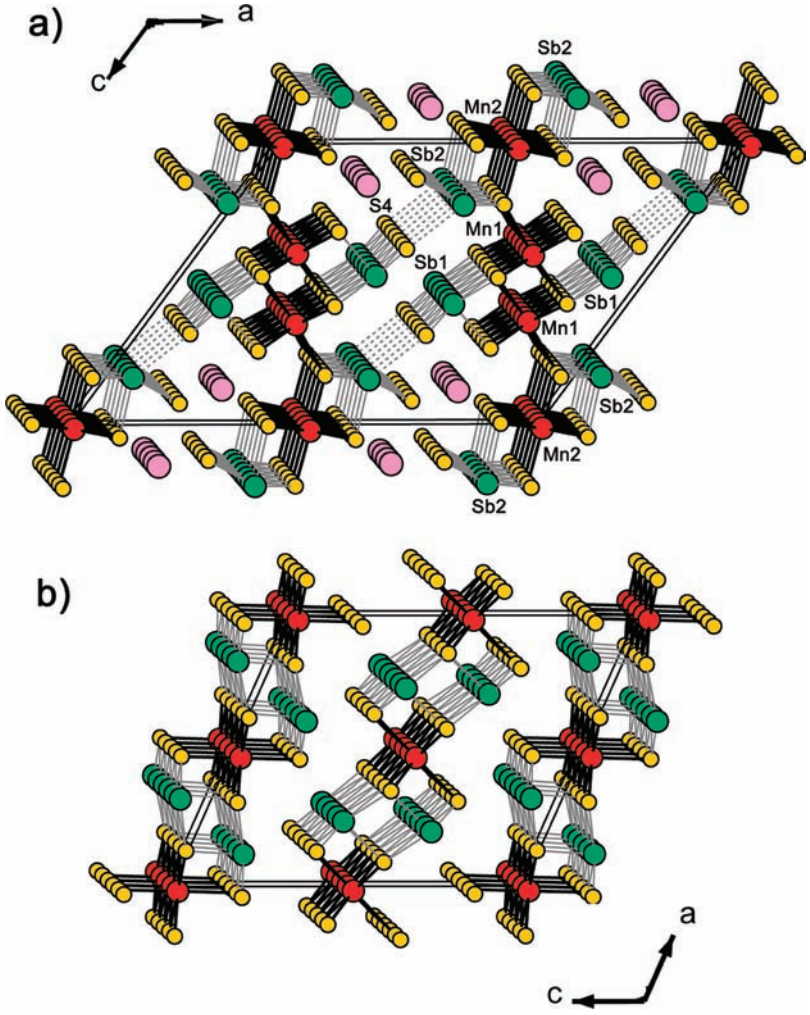

Figure 2. (a) Approximate (010) structure view of $Sm_2Mn_3Sb_4S_{12}$. (b) For comparison, the (0 −1 0) view of $MnSb_2S_4$. Pink, Sm; red, Mn; green, Sb; yellow, S.

gradient approximation with a Hubbard U correction (GGA+U) for the exchange-correlation potentials was used in the calculations.[41,42] A value of 7.5 eV was used for the effective Hubbard U ($J = 0$). The electronic configurations for Sm, Sb, Mn, and S are as follows: Sm, $[Xe]4f^6 6s^2$ (the 4f orbitals are treated as core states in order to converge the self-consistent iterations); Sb, $[Kr]4d^{10}5s^2 5p^3$; Mn, $[Ar]3d^5 4s^2$; and S, $[Ne]3s^2 3p^4$. The values of the atomic radii were taken to be 1.32 Å for Sm, 1.22 Å for Sb, 1.28 Å for Mn, and 1.14 Å for S. Convergence of the self-consistent iterations was performed for 36 k points inside the irreducible Brillouin zone to within 0.0001 Ry with a cutoff of −6.5 Ry between the valence and the core states.

Results and Discussion

Crystal Structure. The four isostructural title compounds feature a new structure type and crystallize in the monoclinic space group $C2/m$ with a = 19.928(2)−19.9672(6) Å, b = 3. 9323(4)−3.8803(2) Å, c = 14.921(2)−14.9011(1) Å, and $Z = 2$ on going from Ln = Pr to Gd, as listed in Table 1. The decrease of the unit cell volume reflects the lanthanide contraction. For simplicity, the structure of $Sm_2Mn_3Sb_4S_{12}$ will be discussed in detail as a representative.

$Sm_2Mn_3Sb_4S_{12}$ characterizes a new wavy MnS_6 octahedron layer decorated on both sides by chains of an SbS_5 square pyramid (Figure 2a). The Sm^{3+} cations are located between such layers with Sm−S distances around 2.93 Å (the normal bond length of Sm−S). Two neighboring Mn/Sb/S layers are also linked through weak Sb2−S4 (~3.06 Å) interactions (indicated by dashed lines in Figure 2a). Each Mn/Sb/S layer consists of a $[Mn1S_6]_2$ dimer chain along the [010] direction that is interconnected with a $Mn2S_6$- octahedron single chain via sharing vertex S1 atoms to form a layer approximately perpendicular to the a direction (side view: Figure 2a; top view: Figure 3a). On both sides of such a layer, strings of SbS_5 square pyramids are attached via Sb1−S5 = 2.45 Å, Sb1−S6 = 2.93 Å, Sb2−S1 = 2.65 Å, and Sb2−S2 = 2.62 Å bonds. Each $Mn1S_6$ octahedron shares two equatorial S5−S6 edges with two other neighboring $Mn1S_6$ octahedra, and two axial S6−S6 edges with two other neighboring $Mn1S_6$ octahedra to generate the so-called "$[Mn1S_6]_2$ dimer chain" along the [010] direction. Each $Mn2S_6$ octahedron shares two equatorial S2−S2 edges with two other neighboring $Mn2S_6$ octahedra to give the so-called "$Mn2S_6$ octahedron single chain" (Figure 3a).

The only known ternary manganese antimony sulfide, $MnSb_2S_4$,[18] is also a layered compound crystallizing in the same space group $C2/m$. Its formula can be written as

(41) (a) Ong, K. P.; Bai, K.; Blaha, P.; Wu, P. *Chem. Mater.* **2007**, *19*, 634. (b) Hinuma, Y.; Meng, Y. S.; Kang, K. S.; Ceder, G. *Chem. Mater.* **2007**, *19*, 1790.
(42) (a) Etz, C.; Stoeffler, D. *Eur. Phys. J. B.* **2006**, *54*, 429. (b) Mestnik, J.; Pereira, L. F. D.; Lalic, M. V.; Carbonari, A. W. *Physica B* **2007**, *389*, 73.

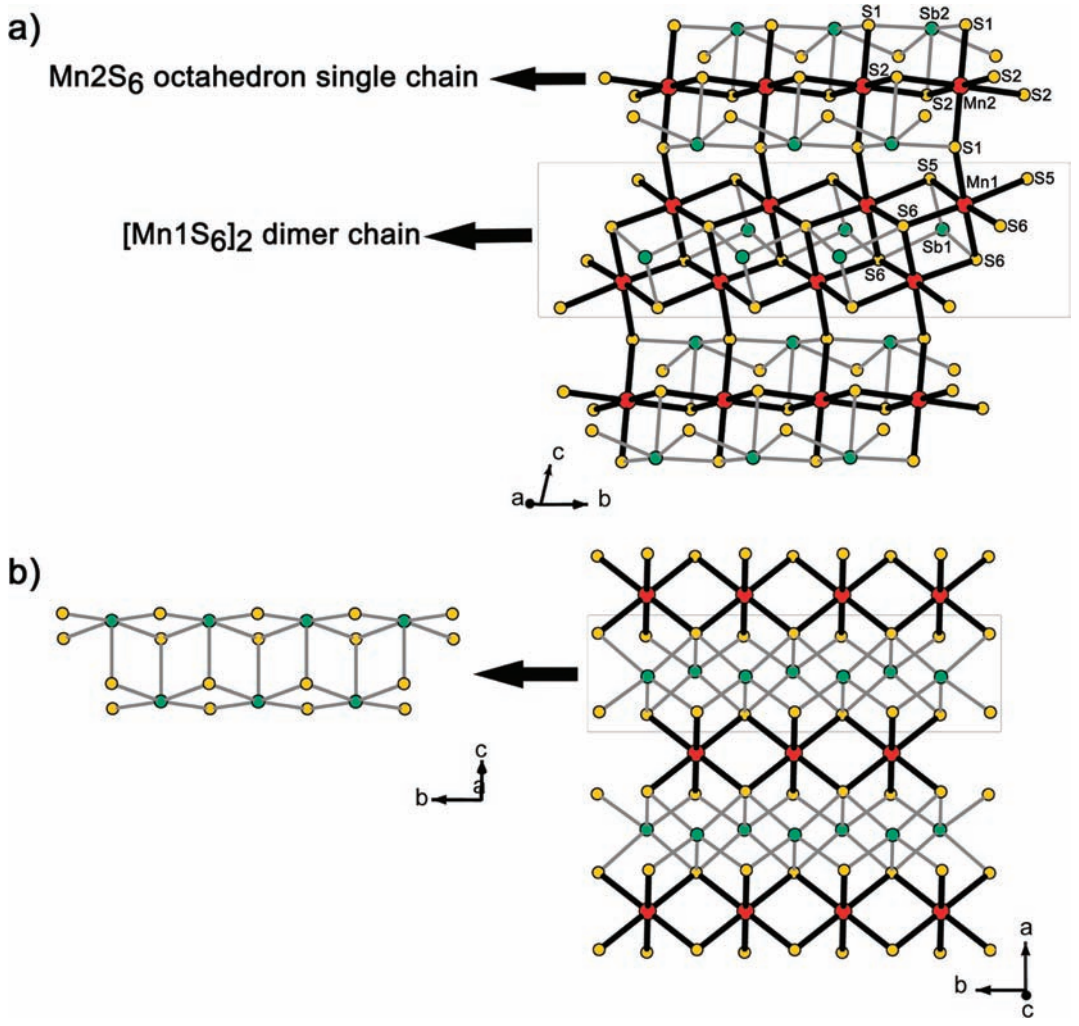

Figure 3. (a) Wavy MnS_6 octahedral layer decorated by chains of an SbS_5 square pyramid in $Sm_2Mn_3Sb_4S_{12}$. The S4 atoms that bridge Sb1 atoms are omitted for clarity. (b) For comparison, the corresponding Mn/Sb/S slab in $MnSb_2S_4$. Red, Mn; green, Sb; yellow, S.

"$Mn_3(Sb_4Sb_2)S_{12} \equiv Sb_2Mn_3Sb_4S_{12}$", which seems to be related to the title compound $Sm_2Mn_3Sb_4S_{12}$. However, a simple comparison will suggest that they are structurally very different, because "Sb_2" is very different from "Sm_2" in many aspects, such as atomic radii, oxidation state, chemical property, bonding ability, and local coordination environment. Crystallographic studies show that, except having the same primary building units, the SbS_5 square pyramid and MnS_6 octahedron, $Sm_2Mn_3Sb_4S_{12}$ and $MnSb_2S_4$, are indeed totally different in terms of packing and connection of the building units, as shown in Figures 2 and 3. The major differences are (1) a $[MnS_6]_2$ dimer chain in $Sm_2Mn_3Sb_4S_{12}$ (as highlighted in Figure 3a) versus the MnS_6 octahedron single chain in $MnSb_2S_4$ (Figure 3b) and (2) a single SbS_5 square pyramid chain in the former versus a double SbS_5 square pyramid chain in the latter (highlighted in Figure 3b). Obviously, the involvement of the lanthanide cation initiates these differences.

On the other hand, both $La_4FeSb_2S_{10}$[26] and $Sm_2Mn_3Sb_4S_{12}$ are layered structures, but the layers are in very different motifs. In $La_4FeSb_2S_{10}$, the FeS_4 and SbS_4 building units belong to different layers, La/Fe/S or La/Sb/S slabs, respectively,[26] while in $Sm_2Mn_3Sb_4S_{12}$, MnS_6 and SbS_5 together construct the same wavy octahedron−square pyramid layer described above.

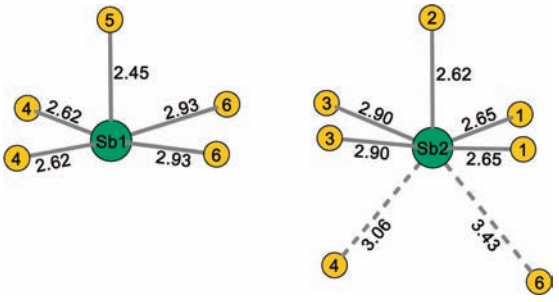

Figure 4. Local coordination environments of Sb atoms in $Sm_2Mn_3Sb_4S_{12}$.

There are two independent Sb atoms, Sb(1) and Sb(2). The Sb(1) is 5-fold coordinated by S atoms in a distorted square pyramid (Figure 4) with three short Sb−S bonds of 2.45, 2.62, and 2.62 Å and two long Sb−S bonds of 2.93 Å, which closely resembles the coordinate environment of Sb in $MnSb_2S_4$,[18] where the Sb's comprise three short bonds between 2.47 and 2.58 Å and two long ones at 3.04 Å. Similarly, the distortion around the Sb(2) centered square pyramid is more obvious, and the Sb2−S bonds range from 2.62 to 2.90 Å, and there are two very weak Sb2−S contacts, as the dashed line indicates in Figure 4. The Sb2−S4 = 3.06 Å bonds are also marked as dashed lines

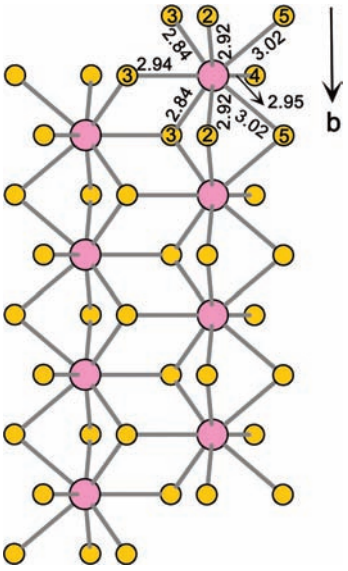

Figure 5. Double chains of SmS_8 bicapped trigonal prisms in $Sm_2Mn_3Sb_4S_{12}$.

in Figure 2a, which correspond to the interlayer weak contacts between the Mn/Sb/S slabs. Such a local environment of Sb2 can be described as a monocapped trigonal prism (Figure 4), as observed in Sb_2S_3, where Sb forms three short Sb−S bonds varying from 2.46 to 2.68 Å, two intermediate distances of 2.85 Å, and two very weak contacts of 3.38 Å.[43]

The two distinct Mn atoms are surrounded by six S atoms with Mn−S distances from 2.43 to 2.78 Å, which are very close to those found in $MnSb_2S_4$, where the Mn−S ranges from 2.55 to 2.64 Å.[18]

The only independent Sm atom is stabilized in a bicapped trigonal prism (BTP) of S atoms that are stacking on top of each other, sharing the trigonal face along the *b* axis and edges with another neighboring BTP SmS_8 string to make an infinite double chain, as indicated in Figure 5. Such a double chain is also found in $BaLaBi_2S_6$.[19] The mean of the Sm−S bonds (2.93 Å) is in good agreement with that in $BaSm_2FeS_5$ (2.93 Å).[44]

Magnetic Properties. $Sm_2Mn_3Sb_4S_{12}$ obeys the Curie−Weiss law at high temperatures with deviations below 60 K (Figure 6). The parameters obtained from the fitting are the Curie constant (C) = 14.33 emu K/mol and the Weiss temperature (θ) = −221.92 K. The theoretical total effective magnetic moment in the temperature region of $T > 60$ K can be calculated by the equation $\mu_{eff}(\text{total}) = [2\mu_{eff}(\text{Sm})^2 + 3\mu_{eff}(\text{Mn})^2]^{1/2} = 10.32\ \mu_B$,[45] which is comparable with the experimental effective magnetic moment, 10.71 μ_B. The negative θ value suggests significant antiferromagnetic (AF) interactions existing between the magnetic ions. Around 6 K, a rapid increase of the susceptibility as shown in the insert of Figure 6 indicates a ferrimagnetic or

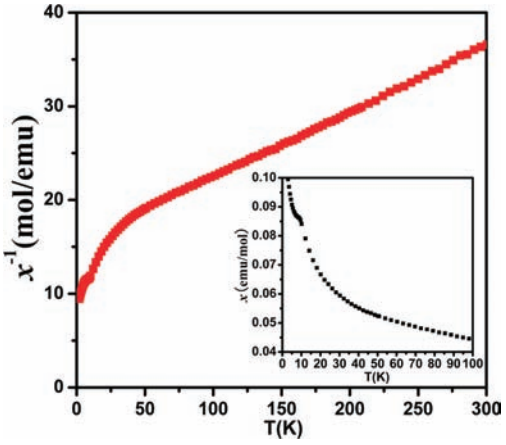

Figure 6. Inverse magnetic susceptivities plotted against temperature for $Sm_2Mn_3Sb_4S_{12}$. Inset: magnetic susceptibility of the temperature below 100 K.

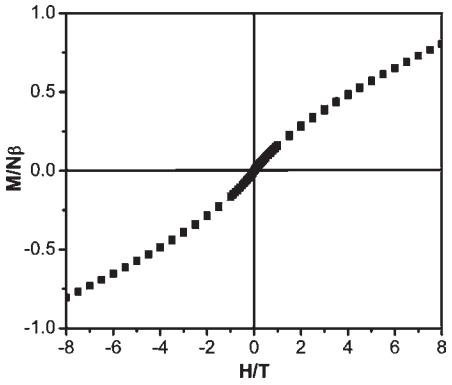

Figure 7. Isothermal magnetization at 2 K versus applied field for $Sm_2Mn_3Sb_4S_{12}$.

a spin-canting AF behavior.[46] As shown in Figure 7, the nonlinear M−H behavior at 2 K reveals the presence of a net magnetic moment. But the field dependence of the magnetization does not follow a Brillouin curve, and magnetization increases to 0.85 Nβ without saturation up to 8T, much less than the common value of 25 Nβ for two Sm and three Mn centers, which suggests a spin-canted AF interaction between the magnetic ions. Such a behavior is also observed in some Mn-containing compounds.[46] The magnetic interactions should happen mainly between the hetero cationic centers $Sm^{3+}-Mn^{2+}$ as well as between the mono cationic centers, $Sm^{3+}-Sm^{3+}$ or $Mn^{2+}-Mn^{2+}$. The shortest Mn−Mn, Sm−Sm, and Sm−Mn distances are 3.51, 3.90, and 3.92 Å. We had tried to synthesize the isotypic "$La_2Mn_3Sb_4S_{12}$" for the magnetic property comparison because the La analogue would naturally only process the magnetic response from the Mn centers. Unfortunately, we only get the known $La_7Sb_9S_{24}$ phase as the main product.[17] We could not obtain the pure phased samples of the other three $Ln_2Mn_3Sb_4S_{12}$ compounds (Ln = Pr, Nd, Gd); the impurity Sb_2S_3 in each sample was irremovable by the methods mentioned above.

Optical Properties. The optical band gap of $Sm_2Mn_3Sb_4S_{12}$ has been measured by the diffuse-reflectance spectra at room temperature as shown in Figure 8. The optical band gap is estimated to be 1.50 eV that agrees with its dark red color. This band gap is smaller than those of binary Sb_2S_3 (1.7−1.9 eV),[27] and MnS (3.2 eV),[30] wider than that of $La_4FeSb_2S_{10}$ (1.00 eV),[26] and comparable

(43) Kyono, A.; Kimata, M.; Matsuhisa, M.; Miyashita, Y.; Okamoto, K. *Phys. Chem. Miner.* **2002**, *29*, 254.
(44) Ino, K.; Wakeshima, M.; Hinatsu, Y. *Mater. Res. Bull.* **2001**, *36*, 2207.
(45) West, A. R. *Solid State Chemistry and Its Applications*; John Wiley & Sons: Chichester, U.K., 1984.
(46) (a) Gao, E.-Q; Yue, Y.-F.; Bai, S.-Q; He, Z.; Zhang, S.-W; Yan, C.-H. *Chem. Mater.* **2004**, *16*, 1590. (b) Sanz, F; Parada, C; Rojo, J. M; Ruíz-Valero, C. *Chem. Mater.* **2001**, *13*, 1334.

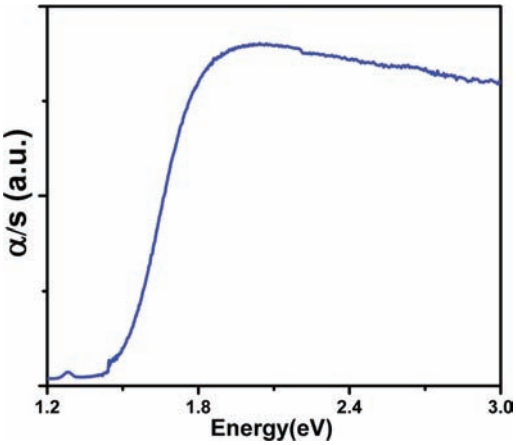

Figure 8. UV−vis diffuse reflectance of $Sm_2Mn_3Sb_4S_{12}$.

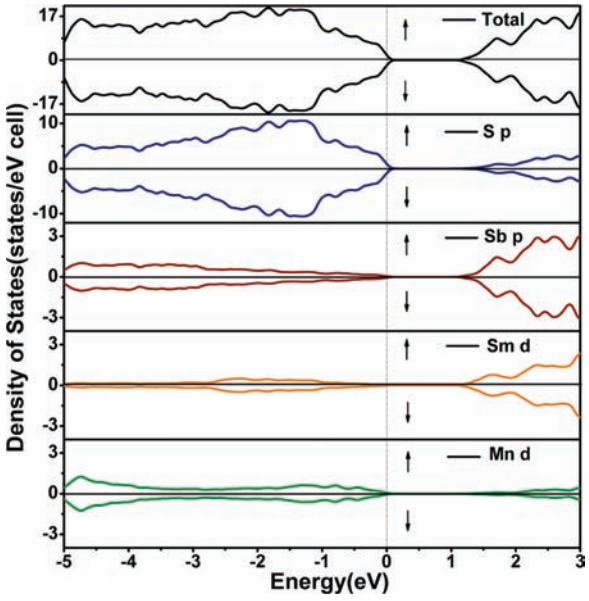

Figure 9. Spin-polarized total and partial densities of states of $Sm_2Mn_3Sb_4S_{12}$.

to that of $La_7Sb_9S_{24}$ (1.55 eV).[17] The essential reason for the band gap difference among these related compounds will be discussed below.

Electronic Structure. In order to understand the distribution of orbitals near the Fermi level, antiferromagnetic (AFM) calculations of the densities of states for $Sm_2Mn_3Sb_4S_{12}$ are shown in Figure 9 (the Sm 4f orbitals are treated as core states in order to converge the self-consistent iterations). The valence band (VB) is dominated by the S 3p block, whereas the conduction band (CB) is primarily Sb 5p and Sm 5d orbital in character, which hybridized with the S 3p orbitals. Note that the contribution from Mn atoms near the Fermi level is almost neglectable, and the Sb 5p orbitals locate at a lower energy region near CB than the Sm 5d orbitals, so the electronic absorption responsible for the optical gap is likely an electronic transfer excitation of S 3p to Sb 5p orbital electrons. The band structure of $Sm_2Mn_3Sb_4S_{12}$ indicates that the VB maximum and CB minimum are located at different k points (Figure 10), and its computational indirect band gap is around 1.06 eV. This value is

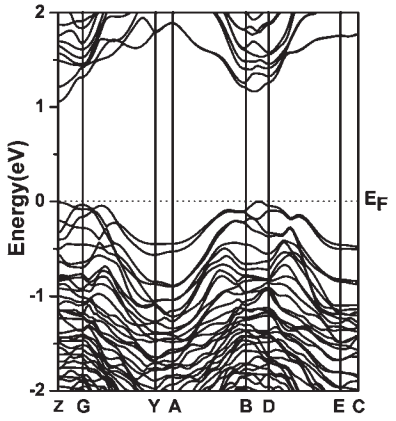

Figure 10. Band structure of $Sm_2Mn_3Sb_4S_{12}$.

smaller than the measured optical band gap, which may be related to the underestimation of the band gap by the DFT method. In comparison, $La_4FeSb_2S_{10}$[26] has a smaller calculated band gap of 0.90 eV, because Fe atoms contribute near the Fermi level and thus reduce the energy of the electronic transfer excitation, that is, an excitation of S 3p-to-Fe 3d orbital electrons in $La_4FeSb_2S_{10}$ with respect to the excitation of S 3p-to-Sb 5p in $Sm_2Mn_3Sb_4S_{12}$, $La_7Sb_9S_{24}$,[17] or Sb_2S_3.[27]

Conclusion

Four new quaternary sulfide indirect band gap semiconductors: $Ln_2Mn_3Sb_4S_{12}$ (Ln = Pr, Nd, Sm, Gd) have been synthesized and characterized. The wavy MnS_6 octahedron−SbS_5 square pyramid layer made by strong Mn−S and Sb−S bonding interactions is unique. Together with our previous work on $La_4FeSb_2S_{10}$, we demonstrated that the local coordination environment and its connection of the transition metal (TM) ions in Ln/TM/Sb/S system are the main reasons for the structural variations; in addition, the involvement of TM ions also leads to new/different properties. The optical band gap of $Sm_2Mn_3Sb_4S_{12}$ is measured to be 1.50 eV, indicating a semiconductor character that agrees with the DFT calculations. An indirect band gap feature is also revealed. $Sm_2Mn_3Sb_4S_{12}$ exhibits spin-canted antiferromagnetic interactions between the magnetic ions. Our further efforts will focus on the introduction of group 13 or 14 elements (T), such as Al, Ga, In, Si, and Ge, into the Ln/Sb/Q (Ln = lanthanide; Q = S, Se, Te) systems; the combination of the TQ_4^{n-} tetrahedron and the acentric SbQ_3^{3-} trigonal pyramid may generate new structures with noncentrosymmetric (NCS) compounds that may show interesting second-harmonic generation (SHG) properties.

Acknowledgment. This research was supported by the National Natural Science Foundation of China under Projects 20773130, 20733003, 20821061, 20973175, and 90922021; the "Key Project from CAS" (KJCX2-YW-H01); the 973 Program (2009CB939801); and the "Knowledge Innovation Program of the Chinese Academy of Sciences" (KJCX2-YW-H20).

Supporting Information Available: An X-ray crystallographic file (CIF), EDX spectrum of $Pr_2Mn_3Sb_4S_{12}$, and point and coordinate tables. This material is available free of charge via the Internet at http://pubs.acs.org.